INSTITUTE OF PHYSICS PUBLISHING PLASMA PHYSICS AND CONTROLLED FUSION

Plasma Phys. Control. Fusion **46** (2004) B367–B380 PII: S0741-3335(04)85815-9

Nonlinear theory of the ablative Rayleigh–Taylor instability

J Sanz[1,3], R Betti[1], R Ramis[2] and J Ramírez[2]

[1] Laboratory for Laser Energetics, University of Rochester, NY 14623, USA
[2] ETSI Aeronáuticos, Universidad Politécnica de Madrid, Madrid 28040, Spain

Received 2 July 2004, in final form 7 September 2004
Published 17 November 2004
Online at stacks.iop.org/PPCF/46/B367
doi:10.1088/0741-3335/46/12B/032

Abstract
Here, a model for the nonlinear Rayleigh–Taylor instability (RTI) of a steady ablation front based on a sharp boundary approximation is presented. The model includes the effect of mass ablation and represents a basic tool for investigating many aspects of the nonlinear ablative RTI relevant to inertial confinement fusion. The single mode analysis shows the development of a nonlinear exponential instability for wave numbers close to the linear cutoff. Such a nonlinear instability grows at a rate faster than the linear growth rate and leads to saturation amplitudes significantly larger than the classical value 0.1λ. We also found that linearly stable perturbations with wave numbers larger than the linear cutoff become unstable when their initial amplitudes exceed a threshold value. The shedding of long wavelength modes via mode coupling is much greater than predicted by the classical RTI theory. The effects of ablation on the evolution of a front of bubbles is also investigated and the front acceleration is computed.

1. Introduction

The Rayleigh–Taylor instability (RTI) has great relevance in inertial confinement fusion (ICF) and astrophysics [1]. In ICF, the low density ablating plasma accelerates the imploding shell inward and the outer shell surface is unstable to the RTI. Mass ablation is caused by the heat front propagating through the shell and driven by the laser energy absorbed at the critical surface.

It has long been known [2] that mass ablation reduces the growth rate of the RT in the linear regime. However, only recently, self-consistent linear theories [3] have identified the stabilization mechanisms in subsonic ablation fronts by using complicated asymptotic matching techniques. Subsonic ablation fronts are characterized by two dimensionless parameters [3]: the Froude number $Fr = V_a^2/gL_a$ and the power index n for thermal conduction,

[3] Permanent address: ETSI Aeronáuticos, Universidad Politécnica de Madrid, Madrid 28040, Spain.

$\kappa_{\mathrm{Sp}} = \bar{K}T^n$, where $\bar{K}$ is a constant and T is the plasma temperature. Here g is the inward target acceleration, L_{a} is the characteristic thickness of the ablation front and V_{a} is the average ablation velocity of the overdense material with density ρ_{a}. The analytical stability analyses are usually based on a single temperature (or one group) diffusive model for the heat transport, i.e. the heat flux is proportional to the temperature gradient, and the thermal conductivity follows a power law of the temperature. These simplifications lead to an analytic solution of the linear stability problem. If the radiated energy is negligible, such as in low-Z materials like deuterium–tritium (DT), the energy is transported mainly by electronic heat conduction [4]. In this case the power index $n = 2.5$ (as given by Spitzer and Harm [5]), and the characteristic thickness of the ablation front is obtained by balancing the enthalpy flux with the heat flux yielding $L_{\mathrm{a}} = 2\bar{K}T_{\mathrm{a}}^n/5\dot{m}_{\mathrm{av}}$ [3], where $\dot{m}_{\mathrm{av}} \equiv \rho_{\mathrm{a}}V_{\mathrm{a}}$ is the average mass ablation rate.

The RTI-stabilization mechanisms can be easily identified for ablation fronts with large Froude numbers ($Fr \gg 1$) which are typical of direct-drive ICF capsules with cryogenic DT ablators. For perturbations with wave number $k = 2\pi/\lambda$, the ablative RT growth rate, γ, can be written as $\gamma \approx \sqrt{kg + (2kV_{\mathrm{a}})^2 - k^2V_{\mathrm{a}}V_{\mathrm{b}}} - 2kV_{\mathrm{a}}$, where kg represents the instability drive, $V_{\mathrm{b}} \equiv V_{\mathrm{a}}\rho_{\mathrm{a}}/\rho_k$ represents the blowoff velocity at the distance $1/2k$ from the ablation front, $\rho_k \equiv \mu_k\rho_{\mathrm{a}} \ll \rho_{\mathrm{a}}$ is the corresponding blowoff density at $1/2k$ and the factor $\mu_k = (2kL_{\mathrm{a}}/n)^{1/n}$ is derived from the isobaric equilibrium profiles. The cutoff wave number is determined by setting $\gamma(k_{\mathrm{c}}) = 0$ yielding $k_{\mathrm{c}}g = k_{\mathrm{c}}^2V_{\mathrm{a}}V_{\mathrm{b}}$ and $k_{\mathrm{c}}L_{\mathrm{a}} \sim [(2/n)/Fr^n]^{1/(n-1)} \ll 1$. This result indicates that the unstable spectrum consists only of modes with long wavelength compared with the ablation-front thickness L_{a}, thus validating the sharp boundary approximation. The stabilizing term $-k^2V_{\mathrm{a}}V_{\mathrm{b}}$ represents the restoring force acting on the spikes which experience a larger heat flux than the bubbles due to their closer proximity to the heat source. This enhanced heat flux leads to a larger blowoff velocity and a stronger 'rocket effect' at the spikes. The overall contribution of the other ablative terms (proportional to kV_{a}) is also stabilizing. They represent the damping effect of vorticity-convection off the ablation front and 'fire polishing'. A simple linear sharp boundary model (SBM) with two incompressible fluids, of densities ρ_{a} and $\rho_{\mathrm{h}} \ll \rho_{\mathrm{a}}$, was developed in [6]. Such a model reproduces the results of the self-consistent linear theory when the interface is approximated by an isotherm, and ρ_{h} is replaced by ρ_k, for each k-Fourier mode of the perturbation. The use of the SBM with this self-consistent closure has proved to be very fruitful in linear theory [7] and, as shown here, a SBM can also be developed to study the RTI deeply nonlinear phase.

In the past few years, several attempts have been made to investigate the features of the nonlinear RTI at accelerated ablation fronts [8]. These theories rely on the weakly nonlinear (quasi-linear) approximation of the classical RTI equations (without ablation). The quasi-linear classical results were extended to the ablative regime by simply replacing the classical linear growth rates with the ablative ones. In this paper, we present several surprising new results obtained from the full nonlinear ablative model of [9]. For example, the weakly nonlinear solution of the ablative model leads to very different conclusions with respect to the earlier quasi-linear theories based on the extension of the classical RTI model. Some of these weakly nonlinear results were already addressed in [9] and later confirmed in [10]. Of greater interest, however, is the highly nonlinear single mode and multimode evolution which can only be studied with a full nonlinear model such as the one presented here. Such a model is derived from first principles and closed with an approximation similar to the closure of the linear SBM. It is applicable to ablation fronts with Froude numbers larger than one (such as those in direct-drive ICF capsules with cryogenic DT ablators). As the model correctly captures the physics of the ablative stabilization, it represents a basic tool to study many physical aspects of the single mode nonlinear ablative RTI as well as to investigate multimode interaction including nonlinear ablation effects.

This paper is organized as follows. In section 2 we summarize and discuss the model equations and the closure presented in [9]. In section 3, the results of the weakly nonlinear theory are described with emphasis placed on the generation of long-wavelength modes via mode coupling. Section 4 is devoted to the deeply nonlinear phase when the RTI bubble velocity saturates. Section 5 is concerned with the finite amplitude instability occurring at a wave number exceeding the linear cutoff, while section 6 describes the multimode results related to the bubble competition and bubble front acceleration.

2. The sharp boundary isobaric model

For simplicity, we consider a planar foil of thickness ℓ, subject to an acceleration g induced by the applied ablation pressure P_{a}: P_{a}, g, V_{a} and ℓ are assumed constant over the characteristic RTI time-scale. Attention is restricted to a region of characteristic thickness $\sim k^{-1}$ about the ablation front, where k is a typical wave number of the interface modulation, and it is assumed that $L_{\mathrm{a}} \ll k^{-1} \ll \ell$. Since the primary stabilizing effect of ablation (rocket effect) occurs [3] for wave numbers satisfying $kg \sim k_2^2 V_{\mathrm{a}} V_{\mathrm{b}}$ (i.e. $\varepsilon_k^2 \equiv k V_{\mathrm{a}}^2/g \sim (2kL_{\mathrm{a}}/n)^{1/n} \equiv \mu_k \ll 1$), we assume that both ε_k^2 and μ_k are small and of the same order of magnitude. We also assume that the unperturbed flow is stationary and one dimensional. The three orthonormal vectors $\vec{e}_x$, $\vec{e}_y$, $\vec{e}_z$, identify the frame of reference moving with the unperturbed ablation front ($y = 0$). In such a reference frame, the one-fluid model equations for an ideal gas including heat conduction [3] can be written in the following form

$$\partial_{\mathrm{t}}\rho + \nabla \cdot (\rho\vec{v}) = 0, \qquad \rho(\partial_{\mathrm{t}} + \vec{v} \cdot \nabla)\vec{v} = -\nabla p + \rho g \vec{e}_y, \tag{1}$$

$$\nabla \cdot \left(\tfrac{5}{2} P_{\mathrm{a}}\vec{v} - \bar{K} T^n \nabla T\right) \approx 0, \qquad P = \rho T \approx P_{\mathrm{a}}, \tag{2}$$

where equations (1) represent the continuity and momentum conservation, while equations (2) represent the isobaric approximation of the energy equation and the ideal gas equation of state. Here, ρ, $\vec{v}$, P and T are density, velocity, pressure and temperature, respectively, $p \equiv P - P_{\mathrm{a}}$ is the perturbed pressure ($|p| \ll P_{\mathrm{a}}$), $\bar{K}$ is a constant. The inertial forces are represented by the effective gravitational acceleration $g\vec{e}_y$ and no motion occurs in the z direction ($\vec{r} = (x, y)$). The first of equations (2) is a well-known simplified form of the energy equation based on the isobaric approximation that relative pressure variations are much smaller than the density and temperature variations. The second of equations (2) is the ideal gas equation of state with the temperature replacing the thermal velocity $T \to 2T/m_{\mathrm{i}}$ for a plasma with ion mass m_{i}. The sharp ablation front is represented by a surface (ablation surface), which may be arbitrarily parametrized, and it is located at $\vec{r} = \vec{r}_{\mathrm{a}} \equiv (\eta(\alpha, t), \xi(\alpha, t))$. Using the large-$n$ limit, the resulting large thermal conductivity in the blowoff region leads to an ablation surface that is approximately isothermal. While the $n \gg 1$ expansion can hardly be justified on the basis that $n = \frac{5}{2} > 1$, it has been shown by several authors that such an approximation leads to very accurate results even when n is finite and equal to $\frac{5}{2}$. The ablation surface separates two regions: a region of cold material with high density ρ_{a} at $y < 0$, and a blowoff plasma with a low density ρ_{h} ($\sim\mu_k\rho_{\mathrm{a}} \ll \rho_{\mathrm{a}}$) and high temperature at $y > 0$. Both the cold and hot regions can be considered unbounded since the RTI develops within a region scaling with the inverse wave numbers ($1/k$) which is assumed to be smaller than both the target thickness and the width of the blowoff region. The solution in the two regions is matched using mass $\dot{m} \equiv \rho\vec{v}' \cdot \vec{n}$, momentum $p\vec{n} + \dot{m}\vec{v}'$ and energy $\frac{5}{2} P_{\mathrm{a}}\vec{v}' \cdot \vec{n} - \bar{K} T^n \nabla T \cdot \vec{n}$ flux conservation; $\vec{t}$ and $\vec{n}$ are the tangent and normal (towards the expanding plasma) unit vectors at the interface, respectively, and $\vec{v}'$ is the fluid velocity relative to it defined as $\vec{v}' \cdot \vec{n} \equiv \vec{n} \cdot \vec{v} - \vec{n} \cdot \partial_{\mathrm{t}}\vec{r}_{\mathrm{a}}$. The momentum flux conservation, along $\vec{t}$ and $\vec{n}$, gives us the continuity of both the tangential velocity, $\vec{v} \cdot \vec{t}$, and $p + \dot{m}^2/\rho \equiv q$, respectively.

2.1. The cold region (D_c)

In this region the thermal transport is small ($kKT_a^n/\dot{m}_{av} \ll 1$) and the flow field is approximately potential $\vec{v}_c = \nabla\phi + V_a\vec{e}_y$, while the density and temperature are constant (ρ_a, $T_a \equiv P_a/\rho_a$). The velocity field must satisfy the boundary condition $\vec{v}_c = V_a\vec{e}_y$ at $y = -\infty$ and equations (1) and (2) yield the Laplace and Bernoulli equations for ϕ. Notice that the perturbed pressure scales as $p \sim \rho_a g k^{-1} \gg \rho_a V_a^2 \sim \dot{m}^2/\rho_a$. Thus, the momentum flux along the normal direction to the interface is approximately equal to the perturbed pressure on the cold side of the interface. Furthermore, since mass is ablated off the interface at a rate $\dot{m}$, the mass conservation at the interface yields $\dot{m} = \rho_a(\vec{v}_c \cdot \vec{n} - \vec{n} \cdot \partial_t\vec{r}_a)$ thus leading to the following form of the Bernoulli and kinematic interface equations:

$$\partial_t\phi + \frac{1}{2}((\nabla\phi|_a)^2 + 2V_a\partial_y\phi|_a) + \frac{q}{\rho_a} - g\xi = 0, \qquad \text{at } \vec{r} = \vec{r}_a, \tag{3}$$

$$\vec{n} \cdot \partial_t\vec{r}_a = \nabla\phi \cdot \vec{n} + V_a\vec{e}_y \cdot \vec{n} - \frac{\dot{m}}{\rho_a}, \qquad \text{at } \vec{r} = \vec{r}_a. \tag{4}$$

The system of equations (3) and (4), yields the position of the interface (ξ) once q and $\dot{m}$ are assigned. Note that by setting $q = \dot{m} = V_a = 0$, equations (3) and (4) reduce to the well-known model of the classical RTI with Atwood number ($A_T = (\rho_a - \rho_h)/(\rho_a + \rho_h)$) equal to unity.

2.2. The hot region (D_h)

In the hot region, the normal component of the momentum flux, q, as well as the ablation rate, $\dot{m}$, must be determined at the interface. The analysis is greatly simplified by using the $n \to \infty$ expansion leading to a solution dominated by the large heat transport ($kKT_h^n/\dot{m}_{av} \gg 1$). Indeed, it can easily be shown that the density and temperature gradients scale as $1/n$ and they can be neglected in the $n \to \infty$ limit yielding an approximately flat density and temperature profiles. Due to the large values of n, the temperature gradients are only retained in the expression of the heat flux ($\sim\bar{K}T^n\nabla T \sim \bar{K}T\nabla T^n$). While the density in the hot region is much smaller than in the cold region ($\rho_h \sim \mu_k\rho_a \ll \rho_a$), and the velocity, v_h, is much larger than in the cold region ($v_h \sim \dot{m}_{av}/\rho_h \gg v_c \sim \sqrt{g/k}$), the perturbed pressures are of the same order of magnitude. Additional simplifications of the hot region equations can be made by noticing that the characteristic RTI time-scale is $1/\sqrt{kg}$, thus indicating that the time derivatives ($\partial_t \sim O(\sqrt{kg})$) are much smaller than the convective derivatives, $\vec{v}_h \cdot \nabla \sim O(kV_a/\rho_h) \gg \sqrt{kg}$. Observe that the energy equation (2) can be easily integrated yielding the flow velocity $\vec{v}_h = \vec{v}_r + \dot{m}_{av}\nabla\theta/\rho_h$, $\vec{v}_r$ ($\nabla \cdot \vec{v}_r = 0$) being the rotational part and $\theta \equiv 2\bar{K}T^n/5n\dot{m}_{av}$. The rotational component $\vec{v}_r$ is induced by the vorticity ($\omega\vec{e}_z = \nabla \times \vec{v}_r$) convected to the hot region from the ablation front. Using the new expression for $\vec{v}_h$ and the isothermal approximation for the ablation surface, the continuity of the energy flux and the tangential velocity leads to $\vec{v}_r = \vec{v}_c$ at the ablation surface. This result indicates that the rotational part of the velocity remains small compared with the potential part ($= \dot{m}_{av}\nabla\theta/\rho_h$), throughout the hot region. In the next step, $\vec{v}_h$ is substituted into the continuity equation (1). By neglecting both $\partial_t\rho_h$ and $\vec{v}_r \cdot \nabla\rho_h$, one finds the following eigenvalue problem

$$\Delta\theta \simeq 0, \quad (x, y) \in D_h, \qquad \theta(x, y, t)|_a \simeq 0, \quad \partial_y\theta(x, y = \infty, t) \simeq 1, \tag{5}$$

where the second boundary condition in equation (5) corresponds to a uniform flow in the far blowoff region. Then, using the energy conservation through the interface leads to the following expression for the ablation rate

$$\dot{m} \simeq \dot{m}_{av}\nabla\theta \cdot \vec{n}|_a, \tag{6}$$

where $\dot{m}_{\rm av}$ represents the average value of the ablation rate. Notice that because of the faster ablation at the spike with respect to the tips of bubbles, the instability growth is damped. The next step is the integration of the momentum equation (1) along the interface. Using the incompressible approximation, the momentum flux can be written as $q = (\dot{m}^2 - \dot{m}_{\rm av}^2)/2\rho_{\rm h} + \int \dot{m}\omega\,{\rm d}s$, where the second term is an indefinite integral along the interface with s being its arc-length. The leading term, $q_{\rm L} \equiv (\dot{m}^2 - \dot{m}_{\rm av}^2)/2\rho_{\rm h}$, represents the so-called 'rocket effect' which provides a strong stabilizing restoring force on the spikes. The vorticity, entering in the expression of q, can be obtained from the momentum equation together with $\nabla \cdot \vec{v}_r = 0$. A solution for ω can be found by recognizing that the vorticity is mainly convected with the potential part of the velocity ($\propto\nabla\theta$) and therefore is only a function of χ (the harmonic conjugate function of θ, $\dot{m}\,{\rm d}s = \dot{m}_{\rm av}\,{\rm d}\chi$). Then, the vorticity can be determined from the following linear integral equation

$$\int_0^\infty {\rm d}\theta \int_{-\infty}^{\infty} \frac{\omega(\chi)\,{\rm e}^{-({\rm i}k\chi+|k|\theta)}\,{\rm d}\chi}{|\nabla\theta|^2} = \dot{m}_{\rm av} \int_{-\infty}^{\infty} \frac{\nabla\phi|_{\rm a} \cdot ({\rm i}k\vec{n} + |k|\vec{t})}{\dot{m}|k|}\,{\rm e}^{-{\rm i}k\chi}\,{\rm d}\chi, \tag{7}$$

obtained by using the conformal mapping $(x, y) \rightarrow (\chi, \theta)$.

2.3. Closure and ablating surface equations

With the expressions for q and $\dot{m}$ given above, the model is closed except for the fact that the leading term of the rocket effect ($q_{\rm L} \equiv (\dot{m}^2 - \dot{m}_{\rm av}^2)/2\rho_{\rm h}$) contains the density $\rho_{\rm h}$. Effectively the main shortcoming of the model is that it requires additional information associated with the flow structure behind the ablation front. Such information cannot be introduced self-consistently within the frame of a SBM. In the linear SBM ($x \simeq \chi$) the closure is introduced in Fourier space [6, 7] by means of a rule that reproduces the results of the self-consistent linear theory: the constant density $\rho_{\rm h}$ is substituted for $\rho_k \equiv (2kL_{\rm a}/n)^{1/n}\rho_{\rm a}$, for each k-Fourier mode of the perturbation. An extension of this simple rule ($\rho_{\rm h} \rightarrow \rho_k$) in Fourier space to physical space can be derived on the basis of the following considerations. Let $\dot{m} = \dot{m}_{\rm av} + \delta\dot{m}$ represent the local ablation rate, with $\delta\dot{m}(\chi, t)$ representing a small departure from the equilibrium value $\dot{m}_{\rm av}$, and $\delta\dot{m}_k = F(\delta\dot{m}) \equiv \int_{-\infty}^{\infty} \delta\dot{m}\,{\rm e}^{-{\rm i}k\chi}\,{\rm d}\chi$, its k-Fourier transform. Then, the linearized leading-order restoring force, $(\dot{m}^2 - \dot{m}_{\rm av}^2)/2\rho_{\rm h} \approx \dot{m}_{\rm av}\delta\dot{m}\rho_{\rm h}^{-1}$, in Fourier space is substituted for $\delta q_{{\rm L}k} = \dot{m}_{\rm av}\delta\dot{m}_k\rho_k^{-1}$. Thus, in physical space, the perturbed momentum flux can be rewritten as $\delta q_{\rm L}(\chi, t) = \dot{m}_{\rm av}F^{-1}(\delta\dot{m}_k\rho_k^{-1})$, where F^{-1} is the inverse Fourier transform operator. Note that $\delta q_{\rm L}$ can also be expressed as a convolution product ($*$), $\delta q_{\rm L}(\chi, t) = \dot{m}_{\rm av}(\delta\dot{m} * \rho_{\rm bl}^{-1}) \equiv \dot{m}_{\rm av}\int_{-\infty}^{\infty} \delta\dot{m}(\chi', t)\rho_{\rm bl}^{-1}(\chi - \chi')\,{\rm d}\chi'$, where $\rho_{\rm bl}^{-1}(\chi) \equiv F^{-1}(\rho_k^{-1})$. This closure can be extended to the nonlinear case in a crude but physically reasonable way by replacing the linearized ablative term $\dot{m}_{\rm av}\delta\dot{m}$ with its full nonlinear representation $(\dot{m}^2 - \dot{m}_{\rm av}^2)/2$, thus leading to the following expression of the momentum flux $\dot{m}_{\rm av}(\delta\dot{m} * \rho_{\rm bl}^{-1}) \rightarrow (\dot{m}^2 - \dot{m}_{\rm av}^2) * (2\rho_{\rm bl})^{-1} \equiv q_{\rm L}$. This closure equation completes the description of the full nonlinear SBM whose governing equations are summarized below:

$$\vec{n} \cdot \partial_{\rm t}\vec{r}_{\rm a} = \nabla\phi|_{\rm a} \cdot \vec{n} - V_{\rm a}(\nabla\theta|_{\rm a} \cdot \vec{n} - 1), \tag{8}$$

$$\partial_{\rm t}\phi|_{\rm a} + \frac{1}{2}((\nabla\phi|_{\rm a})^2 + 2V_{\rm a}\partial_y\phi|_{\rm a}) = g\xi - (\dot{m}^2 - \dot{m}_{\rm av}^2) * (2\rho_{\rm a}\rho_{\rm bl})^{-1} - V_{\rm a}\int \omega\,{\rm d}\chi, \tag{9}$$

where $\rho_{\rm bl}^{-1}(\chi) \equiv F^{-1}(\rho_k^{-1}) = (2\pi)^{-1}\int_{-\infty}^{\infty} \rho_k^{-1}\,{\rm e}^{{\rm i}k\chi}\,{\rm d}k$, ϕ is the solution of the Laplace equation in the $D_{\rm c}$ region (verifying $\partial_y\phi = 0$ at $y = -\infty$), θ is obtained from equations (5) and ω from equation (7). Note, that in the case of periodic symmetric perturbations with fundamental wave number k, the momentum flux can be written as a Fourier series in the χ-coordinate: $q_{\mathrm{L}} = (2\rho_k)^{-1}\sum_j [\dot{m}^2 - \dot{m}_{\mathrm{av}}^2]_j \cos(jk\chi)/j^{1/n}$, where $[\cdots]_j$ represents the j-Fourier coefficient.

It can be shown that the system of equations (7)–(9) reproduces the linear case [6, 7] yielding the well-known differential equation $\partial_{\mathrm{tt}}\xi_k + 4|k|V_{\mathrm{a}}\partial_{\mathrm{t}}\xi_k + (\rho_{\mathrm{a}}V_{\mathrm{a}}^2k^2/\rho_k)\xi_k - |k|g\xi_k = 0$, for the Fourier component ξ_k of the interface position $\xi(x, t)$, and the vorticity generated at the interface, $\omega = 2\partial_{\mathrm{tx}}\xi(x, t)$.

3. Weakly nonlinear theory

In this section, the weakly nonlinear solution of the ablative RTI model is presented (details about the analytical derivations will be presented in a forthcoming paper). One of the most interesting aspects is the nonlinear generation of higher harmonics. It is well known from the classical RTI theory [11] that during the early nonlinear evolution, the higher harmonics are produced with phases enhancing the spike growth over the bubble growth and initiating the bubble-spike asymmetry. In the ablative RTI, such a physical picture is quite different. In a weakly nonlinear analysis ($\xi = \sum \xi_j \cos(jkx)$) up to third order, the amplitudes of the perturbation fundamental mode ξ_1, second and third harmonics are significantly modified with respect to the classical RTI amplitudes. Starting from a fundamental mode of wave number $k < k_{\mathrm{c}}$, one can determine the amplitudes of the nonlinearly generated second harmonic $2k$ and its feedback on the fundamental contribution leading to

$$\xi_2 \approx \left(\frac{1}{2} - \tilde{k}\right) k\xi_{k\mathrm{L}}^2, \qquad \xi_1 \approx \xi_{k\mathrm{L}} - \frac{(2-\tilde{k})(1-2\tilde{k})}{8(1-\tilde{k})}k^2\xi_{k\mathrm{L}}^3, \tag{10}$$

where $\xi_{k\mathrm{L}}$ is the linear amplitude ($\sim\mathrm{e}^{\gamma t}$) and $\tilde{k} = (k/k_{\mathrm{c}})^{1-1/n}$. In the limit case $k/k_{\mathrm{c}} \to 0$, the results of classical RTI [11] are recovered. It follows from (10), that the occurrence of negative or positive feedback to the fundamental harmonic depends, unlike the classical RTI, on the wave number: the feedback to the fundamental mode vanishes at the critical wave number $\tilde{k} = \tilde{k}_* \equiv \frac{1}{2}$. Besides, looking at the spike, $a_{\mathrm{s}} \approx \xi_{k\mathrm{L}} + \xi_2$, or bubble, $a_{\mathrm{b}} \approx \xi_{k\mathrm{L}} - \xi_2$, amplitudes, the asymmetry of the shape is reduced or even inverted if $\tilde{k} > \frac{1}{2}$, and hence the bubble amplitude is growing faster than the linear theory predicts, unlike the classical RTI. This effect can have dramatic consequences for wave number perturbations close to the cutoff wave number k_{c}. In figure 1, we have plotted the time evolution of the bubble amplitude (both time and amplitude are normalized) obtained by numerically integrating equations (8) and (9). This figure shows the results for several values of the ratio k/k_{c} and for a Froude number equal to 5. The solution was obtained by assigning a small initial perturbation of the type $\xi(x, 0) = a_0\cos(kx)$ and by numerically solving the full nonlinear model. Observe that the bubble amplitude follows the linear solution (also plotted in the figure) in the early stages of its evolution (i.e. the linear phase). After the linear phase, the bubble amplitude grows at a rate slower (for $k < k_*$) or faster ($k > k_*$) than the linear rate and as predicted by the weakly nonlinear results in equations (10). The critical wave number k_* separating the two different types of behaviour, is weakly dependent on the Froude number and approximately equal to $k_* \simeq 0.5k_{\mathrm{c}}$. It is also interesting to observe how modes on different sides of the critical wave number behave during the transition from exponential growth to constant bubble velocity. Before reaching the constant-velocity regime, the bubble amplitude of modes with $k > k_*$ evolves from the linear exponential phase into a nonlinear exponential growth. This effect is clearly noticeable in figure 1 for the case $k = 1.6k_* = 0.8k_{\mathrm{c}}$, where the nonlinear growth rate, γ_{NL}, is about $0.15\sqrt{kg}$. Though smaller than the classical value, such a nonlinear growth rate is significant when compared with the maximum ablative growth rate. Indeed, the maximum linear growth rate [3], $\gamma_{\max}$, is about $0.45\sqrt{gk_{\mathrm{c}}/4}$ for this case, which is quite close to γ_{NL}.

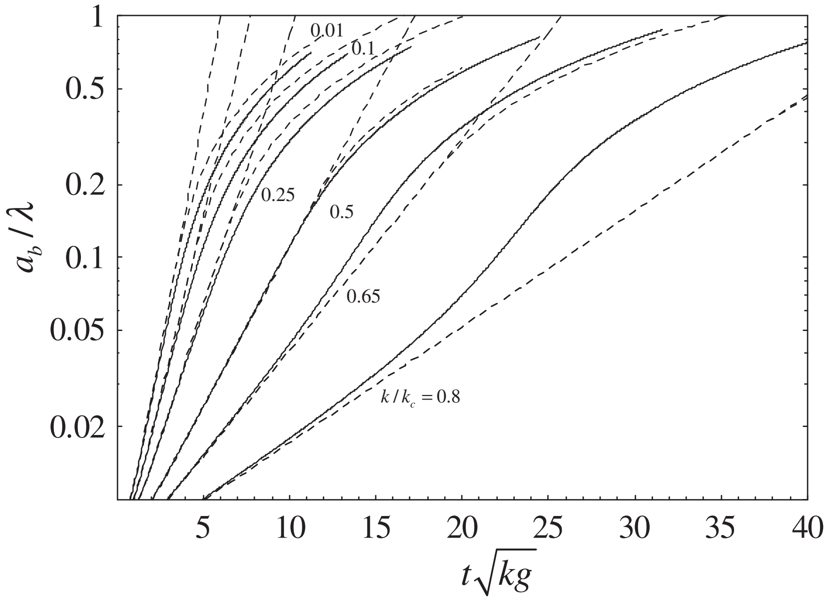

Figure 1. Normalized bubble amplitude versus normalized time, for different values of k/k_c and $Fr = 5$. Solid lines correspond to the full nonlinear results. They were numerically obtained by integrating equations (8) and (9) of the model. Straight dashed lines were obtained from linear theory and curved dashed lines from equations (12) ($a_b = V_b^{\infty}(\gamma^{-1} + t - t_0)$).

The same figure shows that the threshold amplitude for this nonlinear exponential growth is about 0.02λ thus indicating that the linear phase is limited to very small amplitudes $<0.02\lambda$.

Another important aspect of the nonlinear RTI concerns the generation of long wavelength modes via mode coupling. When two modes of wave numbers k_1 and k_2 are initially present, their nonlinear interaction yields the beat mode $k_{12} \equiv |k_1 - k_2|$. The most relevant interaction is the beating of modes with wave numbers about the wave number (k_{op}) for maximum growth rate. A weakly nonlinear analysis up to second order yields the following amplitude of the beat mode, ξ_{12},

$$\xi_{12} = -\left(\frac{k_{12}}{2}\frac{\gamma_2(\gamma_1+\gamma_2)\xi_1\xi_2}{(\gamma_1+\gamma_2)^2 - \gamma_{12}^2}\right) \times A_{abl}, \qquad A_{abl} \equiv 1 + \left(\frac{k_c}{k_{12}}\right)^{1/n} \frac{(1+n)k_1k_2g}{nk_c\gamma_2(\gamma_1+\gamma_2)}, \tag{11}$$

where ξ_1, ξ_2 are the corresponding linear amplitudes, $\gamma_1 = \gamma(k_1)$, $\gamma_2 = \gamma(k_2)$ and $\gamma_{12} = \gamma(k_{12})$. The term in brackets is the classical RTI mode-coupling formula [12] while A_{abl} represents the ablative effects. In the past, the classical formula (equation (11) with $A_{abl} = 1$) was applied to the ablative regime by simply replacing the linear classical growth rates in ξ_1, ξ_2 with the corresponding ablative growth rates. Such a heuristic extension of the classical theory into the ablative regime, is grossly inaccurate since the ablative corrections in A_{abl} are typically large and A_{abl} is often much greater than unity. Indeed, the nonlinear long wavelength generation is strongly enhanced by mass ablation as compared to the classical predictions. This is an important result as long wavelength modes cause macroscopic distortion of the imploding shell leading to non uniform compression of the hot spot and consequent degradation of the target performances. A figure of merit has been identified in the 'mode generation efficiency' defined as $G = -4\xi_{12}/(\xi_1\xi_2k_{12})$. The parameter G provides a good measure of the ablative effects since $G = 1$ in classical RTI (in the limit $k_{12} \to 0$) thus indicating that any significant

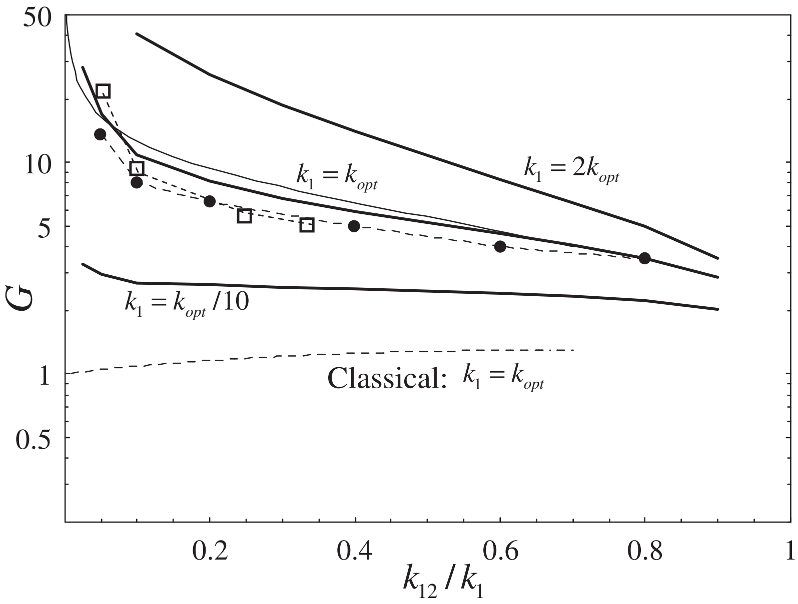

Figure 2. Long wavelength mode generation efficiency (as defined in the text) versus k_{12}/k_1. The thin line corresponds to the weakly nonlinear ablative theory (equation (11)). The thin dashed line corresponds to the weakly nonlinear classical theory. Thick lines were obtained by numerically integrating equations (8) and (9) of the model. Dots correspond to ART simulations, and squares to MULTI two-dimensional simulations.

departure from unity is caused by mass ablation. In order to accurately determine the long wavelength mode generation efficiency, G is inferred from the numerical solution of the full nonlinear model (equations (8) and (9)) and its values are compared with the results of full two-dimensional simulations. Figure 2 shows plots of G versus the dimensionless wave number k_{12}/k_1 for values of $k_1 \simeq 2k_{\mathrm{opt}}$, k_{opt}, $k_{\mathrm{opt}}/10$ and $Fr = 5$. It is important to notice that the long wavelength mode generation efficiency is much larger than in the classical case. Such a result is particularly important when applied to the beating of modes about the wave number of maximum growth rate k_{opt} which is expected to dominate the linear phase. Note that for $k_1 = k_{\mathrm{opt}}$, the long wavelength generation efficiency G can be one order of magnitude higher than predicted by the classical formula. Also, observe that in the limit $k_{12}/k_1 \to 0$, G diverges, in agreement with the analytical result of equation (11), where $G \propto k_{12}^{-1/n}$ ($n = 5/2$). Figure 2 also shows the analytic formula for G given in equation (11) (thin solid line) and its corresponding classical value (dashed line) from equation (11) with $A_{\mathrm{abl}} = 1$. Furthermore, the results of full two-dimensional simulations carried out with the codes ART (dots) and MULTI (squares) confirm the accuracy of the theoretical results. Both ART [13] and MULTI [13] are two-dimensional Eulerian codes solving the hydrodynamic equations including electronic heat conduction. Numerical solutions of the full nonlinear model show that G is only weakly dependent on the Froude number thus indicating that the results in figure 2 can be applied to most cases of interest to direct-drive ICF.

4. Asymptotic bubble velocity

The nonlinear model is also applied to determine the RTI deeply nonlinear phase when the bubble velocity saturates and the amplitude growth turns from exponential to linear in time. Using an analytical approximation similar to the one adopted in [14] for the classical RTI, the ablative model equations (8) and (9) can be solved for the asymptotic bubble velocity yielding $V_{\mathrm{b}}^{\infty} \approx \sqrt{g/3k} - V_{\mathrm{a}}$. Such a result has also been confirmed by the numerical solution of equations (8) and (9). It is important to notice that $\sqrt{g/3k}$ is the Layzer asymptotic bubble velocity for classical RTI [14] while V_{a} is the average ablation velocity representing the average motion of the ablation surface. It follows that the bubble penetration velocity with respect to the unperturbed target material is equal to the classical value $\sqrt{g/3k}$. This result is particularly important since it suggests that the ablative RTI behaves like the classical in the deeply nonlinear regime regardless of the size of the ablative damping in the linear regime. Furthermore, bubbles with wavelength $\lambda < 6\pi V_{\mathrm{a}}^2/g$ are smoothed out by ablation. A simple estimate of the bubble amplitude, a_{b}, in the nonlinear regime can be obtained by instantaneously switching the nonlinear evolution from exponential growth to constant bubble velocity at a time t_0 in which the linear velocity equals the asymptotic bubble velocity

$$a_{\mathrm{b}} \simeq \begin{cases} a_0 \mathrm{e}^{\gamma t}, & (t < t_0), \\ V_{\mathrm{b}}^{\infty}(\gamma^{-1} + t - t_0), & (t > t_0), \end{cases} \tag{12}$$

where $t_0 \equiv (1/\gamma)\log(V_{\mathrm{b}}^{\infty}/\gamma a_0)$. Here, the term $S(k) \equiv \gamma^{-1} V_{\mathrm{b0}}$ is usually referred to as the saturation amplitude for one single mode. The classical saturation amplitude of 0.1λ is recovered in the long wavelength limit $k/k_{\mathrm{c}} \to 0$. However, shorter wavelength modes well into the ablative regime exhibit a saturation amplitude that is significantly larger than the classical prediction [15]. Indeed, saturation amplitudes of 0.15λ and 0.2λ can easily be reached by modes with wave number beyond the wave number for maximum growth rate ($k > k_{\mathrm{opt}}$). This result is particularly important in light of the fact that the output of one-dimensional ICF implosion simulations are commonly post-processed using Rayleigh–Taylor models based on the classical linear saturation amplitude of 0.1λ. The simple estimate in equation (12) is shown in the dotted curves of figure 1 and seem to be in reasonable agreement with the full nonlinear solution for $k < 0.6k_{\mathrm{c}}$. For wave numbers closer to the cutoff wave number, the numerical solution indicates a dramatic increase in the saturation amplitude and the formulae in (12) severely underestimate the saturation amplitude. This discrepancy is caused by the development of the nonlinear exponential growth which becomes much faster than the linear growth as the wave number approaches the cutoff.

5. Finite amplitude instability after the linear cutoff

Another interesting result of the nonlinear theory is the discovery of a new instability for wave numbers beyond the linear cutoff. Modes with $k > k_{\mathrm{c}}$ are linearly stable, i.e. an infinitesimally small perturbation would decay exponentially in time. However, the solution of the nonlinear model reveals that a sinusoidal perturbation with $k > k_{\mathrm{c}}$ can be driven unstable when its amplitude exceeds a critical value. This can be shown through a weakly nonlinear analysis of the nonlinear equations. Setting $\partial_{\mathrm{t}} = 0$ in (8) and (9), and expanding $\xi_{\mathrm{e}}(x) = \sum \xi_{\mathrm{e}j}\cos(jkx)$, the quasi-linear approximation close to k_{c} yields the equilibrium amplitudes $\xi_{\mathrm{e}j}$ for $\tilde{k} > 1$: $\xi_{\mathrm{e1}} \approx \pm k^{-1}(\tilde{k} - 1)^{1/2}$, $\xi_{\mathrm{e2}} \approx -k\xi_{\mathrm{e1}}^2/4$, etc. Obviously such a bifurcated equilibrium is unstable and perturbations with $k > k_{\mathrm{c}}$ can be destabilized if their initial amplitude exceeds the threshold value $|k\xi_1(0)| > \sqrt{\tilde{k} - 1}$. Such a finite-amplitude instability is suppressed when the mode wave number exceeds a critical value denoted as the 'super-cutoff'. The expression for the 'super-cutoff' can be easily extracted from the asymptotic bubble velocity, $V_{\mathrm{b}}^{\infty} = \sqrt{g/3k} - V_{\mathrm{a}}$, indicating that bubbles with wave numbers $k > k_{\mathrm{sc}} \equiv g/3V_{\mathrm{a}}^2$ are smoothed out by ablation. Hence, any surface perturbation with $k > k_{\mathrm{sc}}$ must be stable

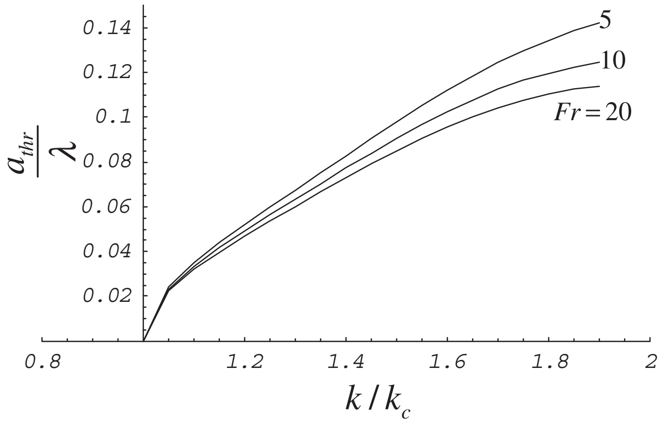

Figure 3. Normalized threshold amplitude for the nonlinear instability beyond k_c versus the ratio k/k_c, for several values of the Froude number.

(linearly and nonlinearly) regardless of its amplitude. Both the development of the finite-amplitude instability as well as the presence of the super-cutoff have been confirmed by the numerical solutions of equations (8) and (9) and by full two-dimensional simulations using the code ART. The threshold amplitude, a_{thr}, for the finite-amplitude instability is plotted in figure 3 versus k/k_c and $Fr = 5$, 10 and 20. A single mode perturbation with an amplitude larger than a_{thr} is unstable. The threshold amplitude vanishes at $k = k_c$, and increases with the wave number till it diverges to infinity for $k \rightarrow k_{\mathrm{sc}}$. Any wave number perturbation beyond k_{sc} is stable regardless of its initial amplitude.

6. Bubble front evolution

When the initial perturbation is made up of multiple modes, the phenomenology of the nonlinear stages differs from the single mode results. In classical RTI theory, if the two fluids (light and heavy) have comparable density ($A_T < 1$), then the RTI is followed by the Kelvin–Helmholtz instability (KHI) which develops from the spikes leading to turbulent mixing between the fluids. In this case, some simple mixing models have been able to provide reliable estimates of the penetration velocity of the fluids and the growth of the mixing region [16]. Oron *et al* [17] derived the asymptotic ablation correction to the classical RT gt^2 mixing zone growth low, in the context of a statistical mechanics bubble-merger model valid for small Froude numbers. However, these models cannot be applied to ablation fronts with large Froude numbers as in direct-drive implosions. In ICF ablation fronts, the densities ratio is typically small, $\rho_h/\rho_a \ll 1$. Hence the flow is mostly laminar and the instability develops a clear structure which remains far from the turbulent regime during the short ICF time-scales. Furthermore, mass ablation off the spike prevents the development of the KHI. Instead, the nonlinear multimode ablative RTI presents many features analogous to the classical RTI with Atwood number unity ($A_T = 1$). Features such as bubble competition and bubble front acceleration have been extensively studied for $A_T = 1$ in classical RTI [18]. Here, we carry out similar analyses for the case of ablative RTI. We first consider the case of an initial array of m bubbles with slightly different wave numbers and approximately equal amplitude. As a result, we expect to observe the development of the 'bubble competition' effect leading to a further enlargement of the widest bubbles at the expense of the shorter ones. Several numerical experiments have been carried out by varying the number of bubbles, wave number and Froude number. Figures 4(*a*) and (*b*) show

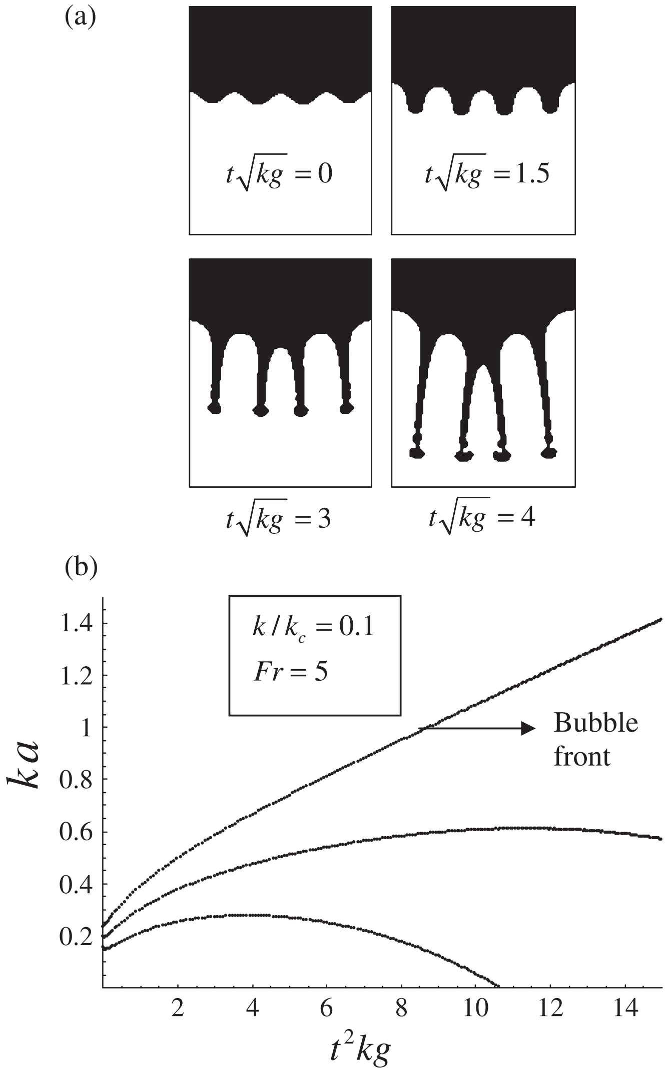

Figure 4. (*a*) Interface position at four different times. (*b*) Normalized location of the tip of bubbles versus normalized time squared.

some representative results with time and length normalized with $\sqrt{kg}$ and k^{-1}, respectively. Figure 4 shows the case of $Fr = 5$ with a box size $\lambda = 2\pi/k$ with $k \simeq k_c/10$, and four initial bubbles ($m = 4$). Four snapshots of the ablation surface are shown in figure 4(*a*). Observe that no noticeable difference in the bubble size develops in the initial stage for $t\sqrt{kg} < 1.5$. The effect of bubble competition becomes apparent later in time when the widest bubble begins moving faster due to the larger space available for its growth. On the other hand, the small bubble moves slowly and shrinks. It eventually disappears after merging with the larger bubbles. In figure 4(*b*), the position of the tips of the bubbles is plotted versus t^2. Notice that the front width, defined as the amplitude of the largest bubble, moves with constant acceleration after the initial stage in which the bubbles are formed. The width of the front h can then be written as $h \simeq \beta g t^2$, where $\beta \simeq 0.06$ for the present case. The case for $m = 8$ and the same

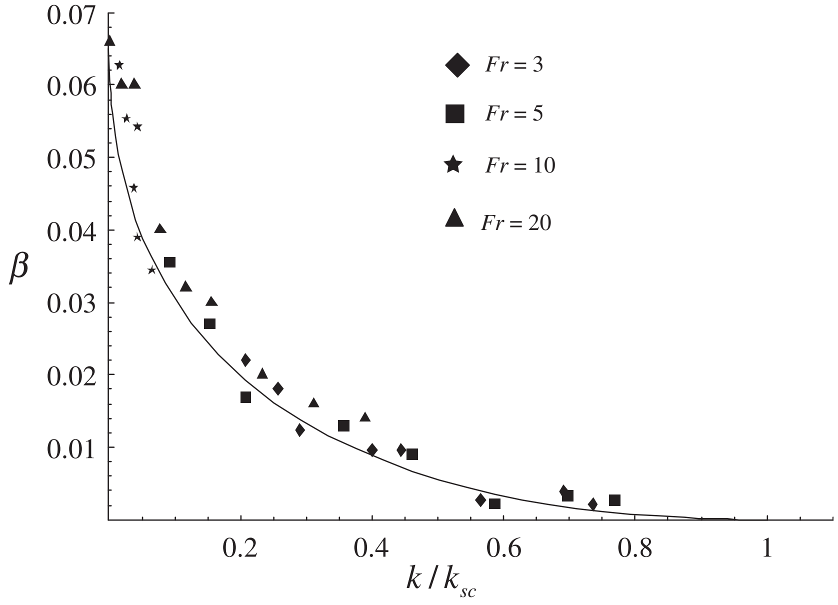

Figure 5. Coefficient β of the bubble front acceleration (♦, ■, ★, ▲) versus normalized wave number for several values of the Froude number. The thin line corresponds to equation (13) ($\beta = \beta_0(1 - \sqrt{k/k_{sc}})^2$).

box wave number k leads to a bubble front advancing with the same constant acceleration, $\beta \simeq 0.06$, as in the case of four bubbles. In order to explore the effects of mass ablation, the box size has been reduced by choosing a box wave number $k = 0.4k_c$. In this case, the four or eight initial bubbles have wave lengths smaller than the cutoff wave length and therefore are linearly stabilized by ablation. However, their initial amplitudes have been chosen to exceed the threshold amplitude for the finite-amplitude instability described in section 5. Thus, the bubbles initially grow in time but the transient towards the bubble-competition regime becomes more intricate. Nevertheless, the bubble front can be clearly identified and its acceleration is still proportional to g. However, the coefficient of proportionality is much smaller than in the previous case and equal to $\beta \simeq 0.03$, regardless of the number of bubbles. Similar calculations performed with $k = k_c$ also show an accelerating bubble front with $\beta \simeq 0.02$.

In summary, different computations with varying box wave number, number of bubbles, Froude number and initial conditions, have all indicated that the bubble front advances with a constant acceleration proportional to g. Although the values of β show a weak dependence on the initial conditions, the following general features can be inferred from the numerical results. The envelope of every number of bubbles (i.e. the bubble front) in a box of a given size $\lambda = 2\pi/k$ advances with the same acceleration. This acceleration reaches the classical value ($\beta \equiv \beta_0 \simeq 0.06$–$0.07$) in the limit $k/k_c \to 0$ where the effects of ablation are negligible regardless of the magnitude of the Froude number. However, for finite values of k/k_c, the bubble front acceleration decreases with k. In fact, if the box wave number exceeds the super-cutoff (defined in section 5), all the bubbles within the box are linearly and nonlinearly stable and the bubble front does not grow. Thus, one can argue that the proportionality constant β is a function of the box wave number normalized with the super-cutoff (k/k_{sc}) and that $\beta = 0$ for $k = k_{sc}$. In figure 5 we show the results of several computations (β versus k/k_{sc}) with Froude number equal to 3, 5, 10 and 20, after a large set of numerical solutions of equations (8) and (9) for different box sizes (i.e. different k) and different number of bubbles. Note that a simple dimensional analysis leads to $h = Ck(V_b^\infty t)^2$ for the amplitude of the bubble front, where V_b^∞ is the asymptotic bubble velocity given in section 4 and C is a constant of proportionality. The latter can be determined by requiring that the bubble acceleration reaches the classical value for $k \to 0$. A simple manipulation yields $C = 3\beta_0$ thus leading to the following final form of the bubble front amplitude

$$h = \beta g t^2 \equiv \beta_0 g \left(1 - \sqrt{\frac{k}{k_{sc}}}\right)^2 t^2 \tag{13}$$

with $k_{sc} = g/3V_a^2$. Observe, in figure 5, the excellent agreement between the formula obtained from (13) and the results of the numerical computations. A qualitatively similar expression was obtained by Oron *et al* [17] for the case of small Froude number.

7. Conclusions

We have described a two-dimensional fully nonlinear model of the ablative RTI including all the relevant physics pertaining to ablation fronts with large Froude number. This model can be applied to investigate the nonlinear evolution of the RTI in direct-drive ICF capsules with cryogenic DT ablators, where the cutoff of the unstable spectrum occurs for long wavelength perturbations compared with the thickness of the ablation front. Several features of the nonlinear stage of the ablative RTI have been discussed. It is found that the long wavelength generation by mode coupling is enhanced by ablation with respect to the classical predictions. Modes with wave number exceeding the linear cutoff are found to become unstable when their initial amplitude exceeds a threshold value. Full stability is only achieved when the wave number is greater than a critical value (larger than the linear cutoff) representing the so-called super-cutoff. Furthermore, linearly unstable perturbations with wave numbers close to the linear cutoff undergo a two-stage exponential growth where the linear stage is followed by a faster nonlinear exponential growth. For the bubble, the exponential growth saturates when the bubble reaches a constant velocity phase where the bubble tip penetrates into the heavy fluid at the classical velocity $\sqrt{g/3k}$. In addition to the single mode results summarized above, multimode analyses have been carried out. The most interesting results concern the effect of ablation on the evolution of the bubble front originated from an initial set of similar bubbles within a fixed computational box. It is found that the bubble front h accelerates with a constant acceleration proportional to g ($h = \beta g t^2$). Differently from the classical results, the constant of proportionality β depends on the box size and vanishes when the box wave number equals the super-cutoff. In summary, the nonlinear model presented here is a valuable tool to study many physical aspects of the ablative RTI and can also be used to carry out more quantitative assessments of the ablative effects on the RTI evolution in direct-drive ICF implosions.

Acknowledgments

JS acknowledges the hospitality of the LLE. This research was supported by the CICYT of Spain (C97010502, FTN 2000-2048-C0301, FTN 2001-3845), by the EURATOM/CIEMAT association, by the Secretaría de Estado de Educación y Universidades de España (Programa de Sabáticos) and the US Department of Energy Office of Inertial Confinement Fusion under Cooperative Agreement No. DE-FC03-92SF19460.

References

[1] Lindl J D 1998 *Inertial Confinement Fusion* (Springer: New York)
Remington B A *et al* 2000 *Phys. Plasmas* **7** 1641
[2] Nuckolls J H *et al* 1972 *Nature* **239** 139
Bodner S E 1974 *Phys. Rev. Lett.* **33** 761
Manheimer W M and Colombant D G 1984 *Phys. Fluids* **27** 983
Takabe H *et al* 1985 *Phys. Fluids* **28** 3676
Kull H J 1989 *Phys. Fluids* B **1** 170
Bychkov V V, Gol'ber S M and Liberman M A 1994 *Phys. Plasmas* **1** 2976
[3] Sanz J 1994 *Phys. Rev. Lett.* **73** 2700
Betti R, Goncharov V N, McCrory R L and Verdon C P 1995 *Phys. Plasmas* **2** 3844
Goncharov V N *et al* 1996 *Phys. Plasmas* **3** 1402
Betti R, Goncharov V N, McCrory R L and Verdon C P 1996 *Phys. Plasmas* **3** 2122
Sanz J 1996 *Phys. Rev.* E **53** 4026
[4] Betti R, Goncharov V N, McCrory R L and Verdon C P 1998 *Phys. Plasmas* **5** 1446
[5] Spitzer L and Harm R 1953 *Phys. Rev.* **89** 977
[6] Piriz A R, Sanz J and Ibáñez L F 1997 *Phys. Plasmas* **4** 1117
[7] Goncharov V N 1999 *Phys. Rev. Lett.* **82** 2091
Sanz J, Betti R and Goncharov V N 1999 *Laser. Part. Beams* **17** 237
Metzler N, Velikovich A L and Gardner J H 1999 *Phys. Plasmas* **6** 3283
Goncharov V N *et al* 2000 *Phys. Plasmas* **7** 5118
Piriz A R 2001 *Phys. Plasmas* **8** 997
[8] Hasegawa S and Nishihara K 1995 *Phys. Plasmas* **2** 4606
Dunning M J and Haan S W 1995 *Phys. Plasmas* **2** 1669
Ofer D *et al* 1996 *Phys. Plasmas* **3** 3073
[9] Sanz J, Ramírez J, Ramis R, Betti R and Town R P J 2002 *Phys. Rev. Lett.* **89** 195002-2
[10] Garnier J, Raviart P A, Cherfils-Clérouin C and Masse L 2003 *Phys. Rev. Lett.* **90** 185003-1
[11] Kull H J 1986 *Phys. Rev.* A **33** 1957
Jacobs J W and Catton I 1988 *J. Fluid Mech.* **187** 329
[12] Haan S W 1991 *Phys. Fluids* B **3** 2349
Remington B A *et al* 1995 *Phys. Plasmas* **2** 241
[13] ART is a code written by R Betti (betti@lle.rochester.edu) and available from the *Laboratory for Laser Energetics, University of Rochester, Rochester, NY*; MULTI 2D: Ramis R, Meyer-ter-Vehn J, *Report* MPQ174, Max-Planck-Institut fur Quantenoptik
Ramis R and Ramirez J 2004 *Nucl. Fusion* **44** 720–30
[14] Layzer D 1955 *Astrophys. J.* **122** 1
Kull H J 1983 *Phys. Rev. Lett.* **51** 1434
[15] Hann S W 1989 *Phys. Rev.* A **39**
[16] Youngs D L 1984 *Physica* D **12** 32
[17] Oron D, Alon U and Shuarts D 1998 *Phys. Plasma* **5** 1467
[18] Zufiría J A 1988 *Phys. Fluids* **31** 3199–212